TIME REVERSAL EXPERIMENTS IN THE MICROWAVE RANGE: DESCRIPTION OF THE RADAR AND RESULTS

L. Bellomo, S. Pioch, M. Saillard, and E. Spano

Laboratoire de Sondages Électromagnétiques de l'Environnement Terrestre (LSEET), UMR CNRS 6017
Université du Sud Toulon-Var
Bâtiment F, BP 20132, LA GARDE CEDEX 83957, France

Abstract—We present a new RADAR system able to perform Phase Conjugation experiments over the ultrawideband [2–4] GHz. The system is equipped with a transmit/receive linear array made of eight antennas connected to a 2-port Vector Network Analyzer through eight independent couples of digitally-controlled RF attenuators and phase shifters. Thus, each channel can selectively transmit or receive and can as well attenuate and phase shift the RF signal. For each frequency, either the Phase Conjugation or the Decomposition of the Time Reversal Operator (DORT) is applied to the received signal and the appropriate amplitude and phase law is coded into the prototype; the focusing wave is then experimentally re-emitted by the array. The quality of the achieved backpropagation is evaluated both in frequency and time domain: In this sense we can speak of Time Reversal. The excellent agreement between measured and theoretical results validates the potential of our system.

1. INTRODUCTION

The concept of Time Reversal Mirror [1–3] has generated numerous studies in both Acoustics and Electromagnetism in the last decade. Many are the potential applications in non-destructive control, medical imaging, sub-marine acoustics, telecommunications and RADAR. The capacity of these mirrors to focus onto an object is very useful for imaging in random media. It permits to improve the signal-to-clutter ratio and to increase the robustness of imaging algorithms. This has been proved on one hand with synthetic data in case of buried

---

Corresponding author: M. Saillard (marc.saillard@lseet.univ-tln.fr).

objects [4] as well as in a circular scanner configuration [5], and on the other with experimental data to construct a better initial estimate for an inversion algorithm in [6]. Our aim here is to build a prototype that allows us to get the data required by such inversion algorithms and to evaluate its performances.

In Electromagnetism, only a few experiments of Time Reversal (TR) have been performed. Recently, particular attention has been devoted to the application of TR techniques in the ultrawideband regime for telecommunications [7, 8] and for detection of targets in the through-the-wall framework [9, 10]. Generally speaking, two different instrumental approaches can be distinguished among the published experiments. A first set of them has been achieved directly in the time domain with a Digital Oscilloscope and an Arbitrary Waveform Generator. Thanks to the latter, it is relatively easy to experimentally re-transmit the reversed wave. As an example, Lerosey et al. [11] realize TR over a 150 MHz-wide band and in a reverberating medium to spot time compression in the reversed signal. In [12, 13] the prototype is employed with a bandwidth of respectively 2 MHz and 2.7 GHz and comprises only one antenna at transmission and one at reception. Space diversity, intrinsic in a very reverberating medium (such as an indoor environment in telecommunications), supplies here the absence of an antenna array. In a second kind of experiments, the systems work in the frequency domain with a Vector Network Analyzer; the re-transmission is only performed numerically. One ought to rather talk about Phase Conjugation over a given bandwidth and pulse synthesis. In [14] the authors exploit a 10 GHz-wide band with again only one antenna at transmission and one at reception. Nonetheless, thanks to a precise mechanical support, they can be placed at different positions in order to artificially "build" two arrays. Finally, Cresp et al. [15] use a bandwidth of 6.5 GHz with a linear eight-antenna array.

Our contribution consists in proposing a system merging the advantages of both described solutions: A prototype, made of a linear eight-antenna array, working in the frequency domain and capable of experimentally re-transmit the complex conjugate of the received signal within a bandwidth of 2 GHz at S-band. Recording an 8×8 transfer matrix also allows us to apply the DORT (french acronym for Décomposition de l'Opérateur de Retournement Temporel) method [16]. This method, initially applied to ultrasonic waves, has later been studied in the frame of Maxwell equations [17–19] and its behavior with respect to polarization has been understood. DORT method is of particular interest as it tells us how to feed the antenna array to focus selectively onto a target. In case of multiple targets, it is more powerful than TR, which has to be iterated and

which restricts focusing to the brightest target.

The remainder of this paper has four main parts. Initially, we recall a few theoretical aspects of both TR and DORT and we describe our approach to a time-domain DORT version valid under free-space conditions. Then, we describe the hardware we dispose of in our system and its behavior. Finally, we present the results of two experiments that we conducted to validate our prototype: In Section 4 and Section 5 respectively, Time Reversal (UWB Phase Conjugation) and time-domain DORT are performed by experimentally backpropagating the array feeding vectors.

2. THEORY OF TIME REVERSAL INVARIANCE IN WAVE PROPAGATION

In vacuum, each component of the electric field $\mathbf{e}(\mathbf{r}, t)$ satisfies the d'Alembert equation

$$\Delta f(\mathbf{r}, t) - \frac{1}{c^2} \frac{\partial^2 f(\mathbf{r}, t)}{\partial t^2} = 0 \tag{1}$$

where c is the speed of light. The solution of this equation is invariant with respect to a sign change in the time t. In other words, if a function $f(\mathbf{r}, t)$ is solution, then $f(\mathbf{r}, -t)$ is also one. Such a property, known as *time reversal invariance*, is ensured by the absence in Eq. (1) of odd-order time derivatives which would appear if the propagating medium had losses.

In the frequency-domain, denoting by $F(\mathbf{r}, \omega)$ the Fourier transform of $f(\mathbf{r}, t)$, Eq. (1) becomes the Helmholtz equation

$$\Delta F(\mathbf{r}, \omega) + k^2 F(\mathbf{r}, \omega) = 0 \tag{2}$$

satisfied by each component of the complex electric field $\mathbf{E}(\mathbf{r}, \omega)$, with $k = \omega/c$. At a given frequency, since k^2 is real, time reversal invariance is equivalent to *phase conjugation invariance*, therefore both $F(\mathbf{r}, \omega)$ and $F^*(\mathbf{r}, \omega)$ are solutions of Eq. (2).

2.1. Time Reversal and DORT

Consider a discrete distribution of N antennas located at $\mathbf{r}_{\text{ant}} = [\mathbf{r}_1 \ldots \mathbf{r}_N]$ able to measure the electric field $\mathbf{e}(\mathbf{r}_{\text{ant}}, t)$ generated by one or more sources. If each of them stocks the field into a memory and re-radiates it back into the medium after time reversal (last element of the memory is output first) the resulting array field will converge onto the sources that originally created the field. Such an array has been baptized *Time Reversal Mirror* (TRM) [1] and its focusing

capabilities have been experimentally exhibited in both acoustics [20–22] and electromagnetism [11–13].

The main drawback of a TRM is the difficulty of focusing selectively on one among different sources, since the backpropagated wave will naturally "prefer" the most radiating one. If the sources are passive targets and the processed signal is the scattered field, one may iterate the TR process to finally focus onto the brightest one. Nevertheless, in case of targets with similar brightness the number of iterations becomes high.

The solution to this issue has been found with the DORT method [16]. This technique requires the knowledge of the inter-element matrix $\mathbf{k}(t)$ whose element $k_{ij}(t)$ denotes the component of the scattered electric field measured at antenna i when antenna j plays the role of emitter. DORT method is based on the singular value decomposition (SVD) of its Fourier transform, the transfer matrix $\mathbf{K}(\omega)$, which writes as $\mathbf{U}(\omega)\mathbf{\Lambda}(\omega)\mathbf{V}^{H}(\omega)$, where the superscript H stands for conjugate-transpose. At the angular frequency ω the diagonal elements of $\mathbf{\Lambda}(\omega)$ are the singular values, whose hierarchy provides information about the brightness of the targets, and the columns of $\mathbf{V}(\omega)$ are the associated right singular vectors, whose complex amplitudes are to be fed to the array to focus selectively onto each target without any iteration.

2.2. Time-domain DORT

DORT method is inherently a time-harmonic technique. To exploit it over a given frequency range, one can start by applying the SVD to each transfer matrix and retrieve the corresponding singular vectors. Despite the fact that each of them will focus correctly onto the target both the amplitude and phase relationships between them are lost because of the decomposition process. Thus, a *time-domain* DORT technique consisting of pulse synthesis out of the raw monochromatic singular vectors fails.

The amplitude issue is commonly solved by weighting the singular vectors by their respective singular value [23, 24], which helps increasing the signal-to-clutter ratio at the frequencies where the targets diffract the most. For the phase problem some ideas have also been investigated. In inhomogeneous media Yavuz et al. [24] build one big space-frequency matrix, assembling all the single-frequency $\mathbf{K}(\omega)$ together; a SVD of this new matrix leads to coherent frequency singular vectors out of which a time-domain excitation for the antennas is built. A different approach [25] consists, in case the target position is known or can be estimated, in equalizing the phases of each re-emitted time-

harmonic field at this location, since the best space-time focusing will naturally be obtained under these conditions.

In free-space, the solution for a working time-domain DORT is fairly simpler than the previous ones. In the case of a scatterer located at $\mathbf{r}_{\mathrm{obj}}$ and small with respect to the wavelength it has been demonstrated [18, 26] that the jth component of the singular vector $\mathbf{v}_1(\omega)$ associated to the largest singular value can be approximated by the complex conjugate of the Green function $G(\omega, \mathbf{r}_j, \mathbf{r}_{\mathrm{obj}})$ from the jth antenna to the object:

$$\mathbf{v}_1(\omega) \approx \mathbf{G}^*(\omega, \mathbf{r}_{\mathrm{ant}}, \mathbf{r}_{\mathrm{obj}})$$
$$= [G^*(\omega, \mathbf{r}_1, \mathbf{r}_{\mathrm{obj}}) \ \ldots \ G^*(\omega, \mathbf{r}_N, \mathbf{r}_{\mathrm{obj}})]^T \qquad (3)$$

In free-space, the phase of each component of $\mathbf{v}_1(\omega)$ varies linearly with respect to frequency. For its last component, for instance, and with a time dependency expressed by $e^{i\omega t}$, we have

$$\arg[v_{1,N}(\omega)] = k|\mathbf{r}_{\mathrm{obj}} - \mathbf{r}_N|. \qquad (4)$$

Although the SVD produces a unitary-norm and arbitrary phase-shifted version of Eq. (3),

$$\mathbf{v}_1^{\mathrm{SVD}}(\omega) = \frac{\mathbf{G}^*(\omega, \mathbf{r}_{\mathrm{ant}}, \mathbf{r}_{\mathrm{obj}})}{\|\mathbf{G}(\omega, \mathbf{r}_{\mathrm{ant}}, \mathbf{r}_{\mathrm{obj}})\|} e^{i\phi(\omega)}, \qquad (5)$$

where $\phi(\omega)$ is an arbitrary phase, one can enforce the norm to be equal to $\lambda_1(\omega)$ and the phase of the last component to match the value in Eq. (4). For the phase, though, this implies the knowledge of the object position. Alternatively, the phase of the last component can be set to zero all over the bandwidth and the final feeding vector $\tilde{\mathbf{v}}_1(\omega)$ becomes

$$\tilde{\mathbf{v}}_1(\omega) = \lambda_1(\omega) \mathbf{v}_1^{\mathrm{SVD}}(\omega) e^{-i\arg\left[v_{1,N}^{\mathrm{SVD}}(\omega)\right]}. \qquad (6)$$

By modeling the antennas of the array as infinitesimal dipoles of vertical moment, the vertical component of the field impinging on the object after re-emission can be written as

$$E(\omega, \mathbf{r}_{\mathrm{obj}}) \propto \mathbf{G}^T(\omega, \mathbf{r}_{\mathrm{ant}}, \mathbf{r}_{\mathrm{obj}}) \tilde{\mathbf{v}}_1(\omega)$$
$$= \lambda_1(\omega) \|\mathbf{G}(\omega, \mathbf{r}_{\mathrm{ant}}, \mathbf{r}_{\mathrm{obj}})\| e^{-i\arg\left[v_{1,N}(\omega)\right]}, \qquad (7)$$

which gives exactly the same space-time focusing as if we used $\mathbf{v}_1(\omega)$ of Eq. (3) only delayed in time by

$$\Delta t_{\mathrm{foc}} = \frac{k|\mathbf{r}_{\mathrm{obj}} - \mathbf{r}_N|}{\omega} = \frac{|\mathbf{r}_{\mathrm{obj}} - \mathbf{r}_N|}{c}. \qquad (8)$$

Interestingly, this solution might be subject to a different interpretation. $\tilde{\mathbf{v}}_1(\omega)$ can in effect be thought of as the limit of an iterative TR

experience starting with the Nth antenna as only active source. If we call $\mathbf{e}^{(0)}(\omega) = [0\ 0\ \ldots\ 1]^T$, $\forall \omega$, such initial steering vector and use $\langle \mathbf{a}|\mathbf{b}\rangle = \mathbf{a}^H \mathbf{b}$ as definition of complex scalar product between vectors $\mathbf{a}$ and $\mathbf{b}$, the vector to be re-transmitted after $2m$ iterations writes

$$
\begin{aligned}
\mathbf{e}^{(2m)}(\omega) &= \left[\mathbf{K}^H(\omega)\mathbf{K}(\omega)\right]^m \mathbf{e}^{(0)}(\omega) \\
&\approx \lambda_1^{2m}(\omega) \left\langle \mathbf{v}_1^{\mathrm{SVD}}(\omega) | \mathbf{e}^{(0)}(\omega) \right\rangle \mathbf{v}_1^{\mathrm{SVD}}(\omega) \\
&= \lambda_1^{2m}(\omega)\mathbf{v}_1^{\mathrm{SVD}}(\omega)e^{-i\arg\left[v_{1,N}^{\mathrm{SVD}}(\omega)\right]},
\end{aligned}
\tag{9}
$$

which apart from the $2m$th power of $\lambda_1(\omega)$ corresponds exactly to Eq. (6). Furthermore, the iterative TR experiment corresponds to the well-known power method used in mathematics for computing the SVD [27]. If indeed one would trigger the power method iterations with $\mathbf{e}^{(0)}$, the first singular vector would simply be $\tilde{\mathbf{v}}_1$. Borcea et al. [28] implicitly also use the iterative TR approach: Since the columns of $\mathbf{K}(\omega)$ still keep the coherence over frequency which is lost with the SVD, one of them is used as $\mathbf{e}^{(0)}(\omega)$.

As described in Section 3, the medium where our experiences are carried out can approximatively be considered as free-space, validating the use of Eq. (6). Employing the same technique, good results have also been found in [15], although the physical justification had not been given. In cases where the waves propagate in more complex conditions, such as in a waveguide [25], the Green function loses its "linear-phase-over-frequency" property and the proposed solution fails.

3. PROTOTYPE DESCRIPTION

The architecture of our RADAR prototype, shown in Fig. 1, can be split in two functional parts: A High Frequency (HF) section and its control logic. The HF section is built around a 2-port Vector Network Analyzer (VNA) serving both as signal source and receiver. The RF front-end is made of a linear array of 8 UWB antennas plus one more spare antenna working in a multistatic configuration. Antennas are antipodal symmetric Exponentially Tapered Slot Antennas (ETSA), printed on a Duroid substrate of permittivity $\epsilon_r = 2.2$ and dimensions $8\,\mathrm{cm} \times 8\,\mathrm{cm}$; they show very good input impedance matching (SWR < 2) in the $[2\text{–}18]\,\mathrm{GHz}$ frequency band and radiate a vertically-polarized (perpendicular to the plane of Fig. 1) electric field [29]. Antennas based on the same design have also been employed in [9, 15]. The distance between the antennas of the array is set to $5\,\mathrm{cm}$ ($\lambda_0/2$ at $3\,\mathrm{GHz}$) to avoid grating lobes while limiting antenna coupling.

Each array channel is controlled both in amplitude and phase via wideband attenuator/phase shifter (A/Φ) couples driven numerically.
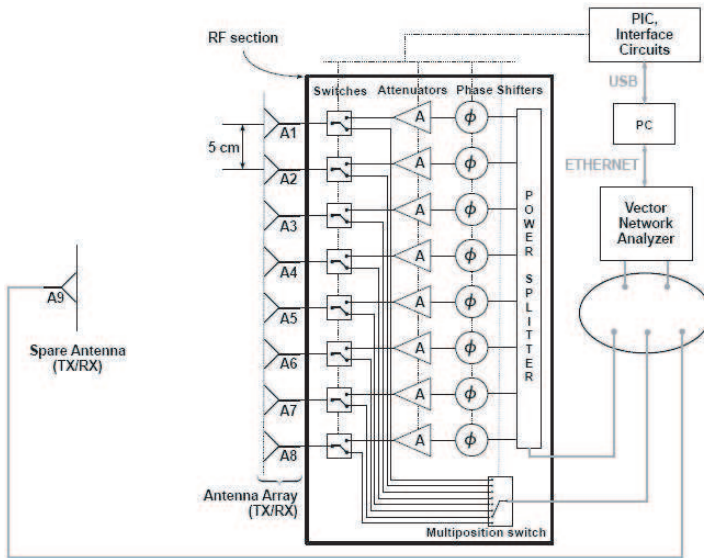
Figure 1. Prototype architecture.

They ensure a dynamic range of respectively more than 30 dB and 360 deg all over the [2–4] GHz frequency band. In order to select any channel combination and direction (transmission/reception), we dispose of an eight-switch bank connected to the antennas and of an additional multiposition switch. Finally, a power splitter allows to recombine/split the eight channels. Since all the RF components are passive elements, the system is reciprocal and can be used both as transmitter and receiver.

In conclusion, three different RF accesses are available: The spare antenna, the power splitter and the multiposition switch. Depending on the targeted experiment, two out of these three points are connected to the VNA. Looking for a compromise between cost, material availability and overall dimensions, our prototype works between 2 and 4 GHz. The low end is imposed by the adaptation of the antennas, the high end by the dynamic range of the phase shifters.

The control of the HF hardware is performed in the PC by a Matlab application. The VNA is driven through an Ethernet link, switches and A/Φ's through a PIC microcontroller connected *via* USB to the PC.

All measurements are carried on in a 1.5 m × 0.6 m chamber made of flat absorbing panels and containing only the antennas and the propagation medium (air). The choice of the VNA frequency step

is based on the total electrical length of the RF paths from port 1 to port 2 of the analyzer, which amounts in the worst-case configuration to a distance of about 12 m (cables, RF components, chamber length, etc.). Taking some margin on this value, the step is set to 10 MHz (201 points in the 2–4 GHz band) which indeed gives an alias-free range of 15 m.

4. TIME REVERSAL EXPERIMENT

4.1. Details of Measurement

The first experiment consists in time-reversing the field radiated by an active source, the spare antenna A_9 in Fig. 1, in the empty chamber. In the first step, called "data-acquisition" and sketched in Fig. 2(a), the array antennas receive the wave radiated from A_9. Since the VNA is 2-port only, we cannot record simultaneously all eight transmission S-parameters. Thus, despite the fact that all the antennas are always
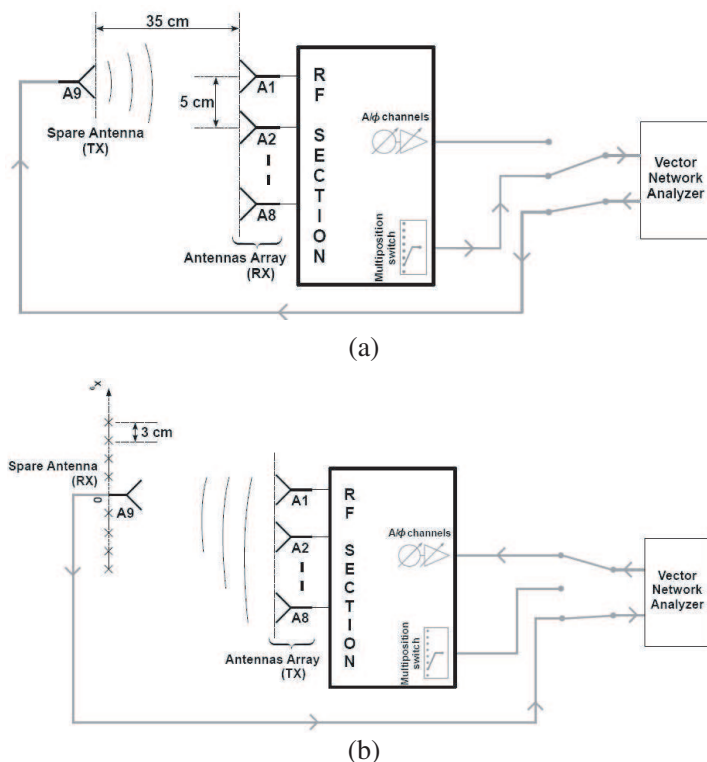

(a)

(b)

Figure 2. Time reversal experiment setup: (a) Data-acquisition and (b) backpropagation steps.

physically present, the acquisition is done sequentially by each of them, selected *via* the switches. Each measurement is denoted by S_{j9}, where j corresponds to the number of the receiving antenna and 9 to the transmitting one. The result is an eight-element vector $\mathbf{S}_{j9} = [S_{j9}]_{j=1,8}$ at each of the 201 frequencies.

Once the acquisition is complete, the array plays the role of transmitter and A_9 that of receiver (Fig. 2(b)). Passing through the power splitter, the signal sent by the VNA reaches all the channels. The eight signals are attenuated and phase shifted selectively before being radiated by their respective antenna. Since our prototype works in the frequency domain, the amplitude/phase law to implement in the A/Φ couples is given by the phase conjugation at each frequency of the acquired data, resulting in the $\mathbf{S}_{j9}^*$ vectors. The received signal at A_9 is then measured by the VNA and the transmission S-parameter, called S_{9A}, is recorded by the PC. To reduce the time needed to cover the whole 2 GHz-wide band, Phase Conjugation is applied with a frequency step of $\Delta f = 100\,\text{MHz}$ (21 points). Finally, the conversion to time domain *via* Inverse Fast Fourier Transform (IFFT) leads to a synthetic pulse equivalent to the result of a true time-domain TR experiment.

Watching carefully at Figs. 2(a) and 2(b), one might notice that the RF signal does not follow the same path when the array acts as transmitter or receiver. In effect, in the data-acquisition step we do not want the received signal to go through the A/Φ channels but rather through the multiposition switch: Since the former path is much more lossy than the latter, the measurement would otherwise suffer from a reduced precision. Now, since reciprocity is not verified under these conditions, $\mathbf{S}_{j9}$ must be transformed at each frequency into a new vector containing the field that would have been measured if the signal went through the A/Φ couples. This is done by using the ABCD matrix multiplication technique [30], made possible thanks to a previous full characterization of each RF channel. Only now experimental Phase Conjugation can be performed.

4.2. Results and Discussion

A first approach to evaluate the quality of the experiment consists in studying amplitude and phase of the measured S_{9A} directly in the frequency domain. We suggest to compare S_{9A} with an ideal reference built from $\mathbf{S}_{j9}$ measured during the data-acquisition step. In effect, Phase Conjugation means feeding the antennas of the array with $\mathbf{S}_{j9}^*$ *because* the measurement associated to the propagation from A_9 to A_j is S_{j9}. Thus, the backpropagated signal finally measured at A_9 in an

ideal case, S_{9A}^{id}, can be written as

$$S_{9A}^{\text{id}} = \mathbf{S}_{j9}^{H}\mathbf{S}_{9j} = \|\mathbf{S}_{j9}\|^{2}, \tag{10}$$

where we have exploited reciprocity ($S_{j9} = S_{9j}$) for the last equality. This equation shows the importance of having the forward and backward signals following the same paths. If this condition does not hold, the $\mathbf{S}_{j9}^{H}$ and $\mathbf{S}_{9j}$ terms would not "compensate" and the reversed field S_{9A}^{id} would not have phase equal to zero. In conclusion, the measured field shall at best equal the result of Eq. (10).
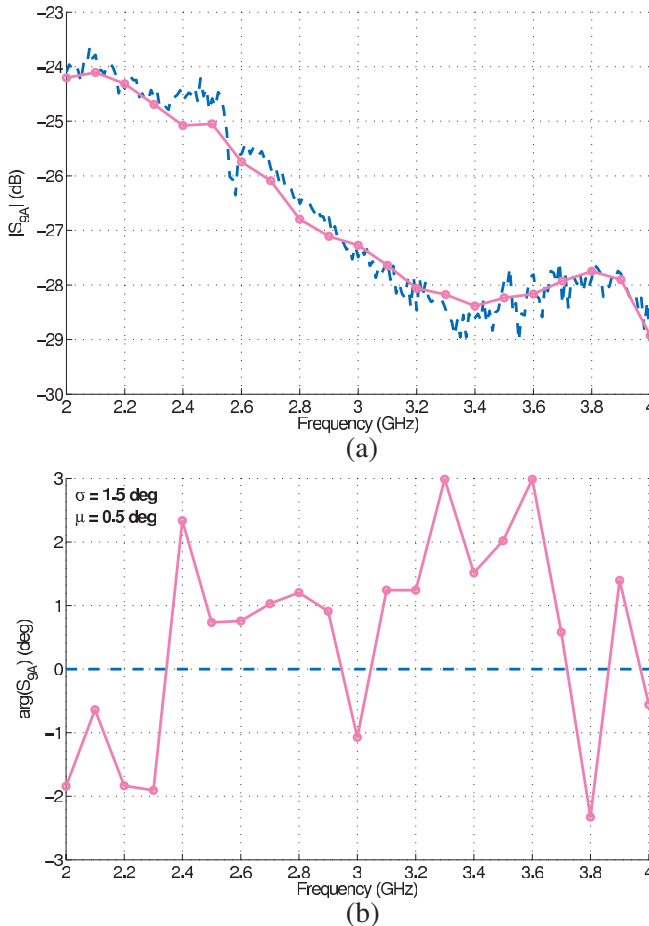

Figure 3. Phase conjugation experiment. Comparison between (a) amplitude and (b) phase of $S_{9A}(\omega)$ in the theoretical and measured cases, respectively in dashed and full line.

The results are presented in Fig. 3. The dashed curve is the reference signal S_{9A}^{id}, while the measurement, normalized in power in order to be comparable to Eq. (10), is shown in full line with circle markers. The measured phase has a mean value of only 0.5 deg and a standard deviation of 1.5 deg. Similarly, the amplitude error never exceeds 1 dB. We can conclude that we have almost perfectly achieved the ideal Phase Conjugation result.

By applying the IFFT to $S_{9A}(\omega)$ (after zero-padding the spectrum bins from 0 to 2 GHz) we synthesize the pulse received by A_9, $s_{9A}(t)$. Since we do not apply any pulse shaping in order to preserve all the spectral information we have, $s_{9A}(t)$ has the shape of a *sinc* pulse of 1 GHz bandwidth (half the operational bandwidth) modulated by a *cosinus* function of frequency 3 GHz (central operational frequency). Furthermore, for a better visualization of the result, we apply the Shannon interpolation formula to the discrete samples to build a "continuous time" version of $s_{9A}(t)$.

Both theoretical (IFFT of Eq. (10)) and measured s_{9A} are depicted in Fig. 4. Again, we remark an excellent agreement between theory and measurement. The experimental signal is not wider in time than the ideal one, and the secondary "lobes" are not higher either, meaning that the time-compression brought related to TR is achieved despite the slightly reverberating character of our chamber (flat absorbers strongly reflect in oblique incidence). This means that at all frequencies
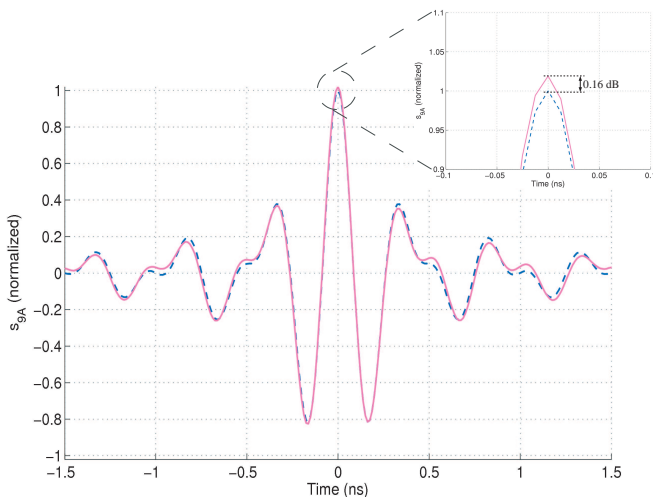

Figure 4. Phase conjugation experiment. Comparison between the IFFT of $S_{9A}(\omega)$ in the theoretical and measured cases, respectively in dashed line and full line with circle markers.

the signals transmitted by the antennas of the array all interfere constructively at the position of A_9. A quantitative indication of the quality of our wideband Phase Conjugation can be found in the ratio between the two signals at the time $t = 0$. In effect, according to the definition of IFFT, this corresponds to a comparison of the coherent sum of the frequency samples of S_{9A} in the theoretical and experimental cases. For our experiment, such ratio is as small as $0.16\,$dB. This residual, and in general the small discrepancies in Fig. 3, can be explained by the discrete resolution of attenuators and phase shifters and by the limited VNA dynamic range.

In order to evaluate the quality of spatial focusing, we have measured the backpropagated field along a line parallel to the antenna array and centered at the original A_9 position, as depicted in Fig. 2(b). While the array is still fed with the Phase Conjugation law at each frequency, A_9 is placed at nine equally spaced spots with a step of 3 cm denoted by the vector $\mathbf{x}_9 = \begin{bmatrix} x_9^{-4} & \ldots & x_9^0 & \ldots & x_9^4 \end{bmatrix}^T$. At each angular frequency ω we obtain

$$\mathbf{S}_{9A}(\omega, \mathbf{x}_9) = \begin{bmatrix} S_{9A}(\omega, x_9^{-4}) & \ldots & S_{9A}(\omega, x_9^0) & \ldots & S_{9A}(\omega, x_9^4) \end{bmatrix}^T. \quad (11)$$

For each position, we use two criteria inspired by Fig. 3, both based on the measurements over the entire bandwidth. First we observe the phase of the new $\mathbf{S}_{9A}$ in the frequency domain. In effect, perfect focusing implies a linear phase law, a particular case of which is the zero slope (Fig. 3(b)). Thus, we have measured the standard deviation $\sigma_{\phi_{\mathrm{err}}}(\mathbf{x}_9)$ of the phase error $\phi_{\mathrm{err}}(\mathbf{x}_9)$ with respect to the linear phase law that best interpolates the measurements, $\arg_{\mathrm{lin\ int}} [\mathbf{S}_{9A}(\omega, \mathbf{x}_9)]$:

$$\begin{cases} \phi_{\mathrm{err}}(\mathbf{x}_9) = \arg [\mathbf{S}_{9A}(\omega, \mathbf{x}_9)] - \arg_{\mathrm{lin\ int}} [\mathbf{S}_{9A}(\omega, \mathbf{x}_9)] \\ \sigma_{\phi_{\mathrm{err}}}(\mathbf{x}_9) = \sqrt{\mathrm{Var}\left[\phi_{\mathrm{err}}(\mathbf{x}_9)\right]} \end{cases} \quad (12)$$

The result is given in Fig. 5(a), where $\sigma_{\phi_{\mathrm{err}}}(\mathbf{x}_9)$ clearly increases for positions away from the original one (0 cm). Also, the faster increase when going towards negative position values is expected because the original position of A_9 is not centered but rather $17.5\,$cm aside with respect to the center of the array.

The other criterion consists in performing the IFFT of $\mathbf{S}_{9A}(\omega, \mathbf{x}_9)$ and keeping the maximum value of the resulting time-domain $\mathbf{s}_{9A}(t, \mathbf{x}_9)$ [31]. For the central position, we already know from Fig. 4 that the maximum occurs at $t = 0\,$ns thanks to phase conjugation and reciprocity of the setup between data-acquisition and backpropagation steps; in the other cases this is in general not true, since the location of A_9 is not the same in the two steps. The resulting normalized amplitudes are shown in Fig. 5(b), which confirms what has already been observed with the phase error standard deviation criterion.
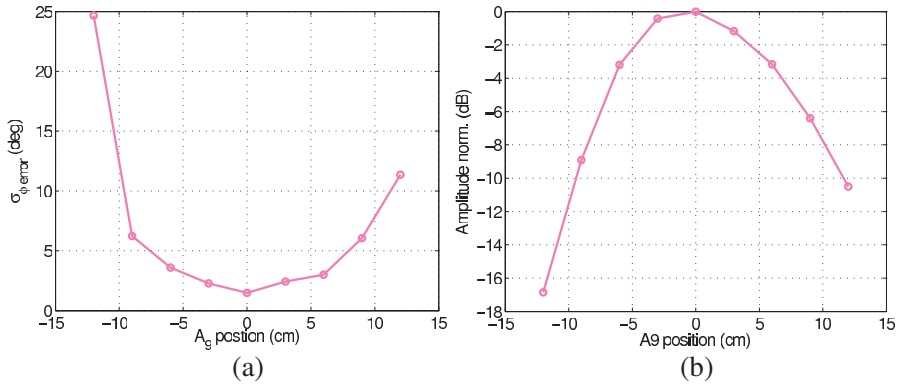
Figure 5. Phase conjugation experiment. (a) Standard deviation of ϕ_{err} and (b) normalized IFFT amplitude maximum as a function of A_9 position.
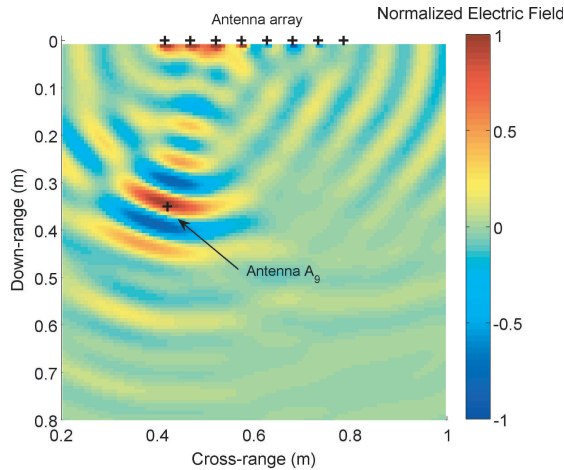

Figure 6. Phase conjugation experiment. Time-domain field chart at the instant when the re-emitted wave focuses on A_9.

A final analysis of the experiment consists in a more classical numerical backpropagation of $\mathbf{S}_{j9}^*$ over the whole frequency range. We model our antennas as infinitesimal dipoles of vertical moment in free-space. This modeling choice introduces an error in the TR process because it adds a mismatch between the characteristics of the antennas in the experimental data-acquisition step and in the synthetic backpropagation, invalidating the reciprocity theorem. Nevertheless, it proves to be rather effective especially because our antennas have

a very stable phase center over the [2–4] GHz bandwidth, exactly as infinitesimal dipoles do. For each frequency we produce a field chart, showing the map of the amplitude of the electric field inside our chamber. Finally, by taking the IFFT of the field values at each pixel, we generate a field chart for every time instant, which allows us to observe the focusing process in the time-domain. Such a chart at the instant where the focusing spot is best concentrated around the position of A_9 is presented in Fig. 6.

5. TIME-DOMAIN DORT EXPERIMENT

5.1. Details of Measurement

In our experiment, the diffracting object is a metallic cylinder placed at a distance of 40 cm from the center of the array (Fig. 7). During the initial data-acquisition step it is illuminated sequentially by each of the array antennas and the field is recorded by all of them. The transfer matrix $\mathbf{K}_{\mathrm{meas}}$ is thus built for each frequency between 2 and 4 GHz. Although the K_{ij} element comprises the propagation of the RF wave not only through the air but also through the jth multiposition switch and the ith A/Φ channel (except for diagonal elements for which the signals pass twice through the multiposition switch), we are only interested in the air part. In order to extract an equivalent $\mathbf{K}_{\mathrm{air}}$ (for the following we will neglect the index "air") we employ the ABCD matrix technique as already mentioned at the end of Section 4.1.

Coupling between antennas, due to their proximity and to their scarce directivity, alters the measurements. The signal received by the selected antenna is indeed the result of both diffracted field coming from the object (useful signal) and direct field coming from the neighbor transmitting antenna (noise). To reduce this unwanted contribution, we actually perform differential measurements [15]. Once the total field matrix $\mathbf{K}^{\mathrm{t}}$ is acquired, the incident field matrix $\mathbf{K}^{\mathrm{i}}$ is
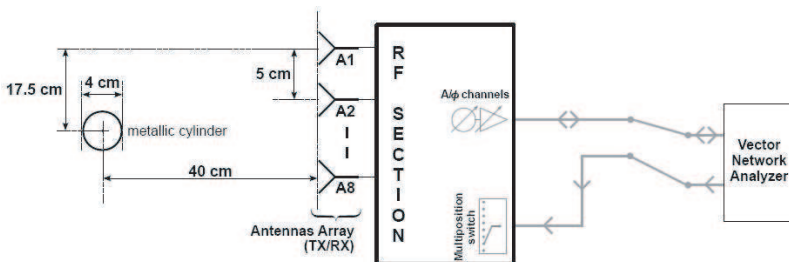

Figure 7. DORT experimental setup.

measured after removing the target. Finally, we retrieve the diffracted field by simple difference:

$$\mathbf{K}^{\mathrm{d}} = \mathbf{K}^{\mathrm{t}} - \mathbf{K}^{\mathrm{i}}. \tag{13}$$

The accuracy of the subtraction is set by the VNA precision. In practice, we manage to reduce the incident field by 25 to 35 dB, hence ultimately setting the dynamic range of our diffraction experiments.

Before applying the SVD to $\mathbf{K}^{\mathrm{d}}$, we convert each of its elements to time-domain by IFFT and apply windowing to remove the very first and last parts of the signal. The first contains most of the antenna coupling residual after subtraction, the last is unnecessary since our absorbing chamber is only 1.5 m long but we dispose of a much "longer" signal due to the 10 MHz frequency step. In practice we cut the first 1.5 ns and keep a 8.5 ns-long window, which means that we can detect objects at a distance from the array going from 22.5 cm up to 1.5 m.

A further conversion back to the frequency domain gives the final $\mathbf{K}^{\mathrm{d}}$ to be decomposed. Time-domain DORT is then applied according to the methodology presented in Section 2.2, giving the focusing singular vector $\mathbf{v}_1$ for each frequency. As for the Time Reversal experiment, the array is now ready to act as emitter, in order to experimentally focus the field onto the target: $\mathbf{v}_1$ is coded in the A/Φ couples and the array transmits. Again, a differential measurement is performed to alleviate the antenna coupling problem. The multiposition switch used during data-acquisition is now useless, since it is the array as a whole that receives the field diffracted by the target. Consequenctly the received signal is again attenuated/phase shifted by the same $\mathbf{v}_1$ law, and in practice we simply measure one reflection S-parameter per frequency called S_{AA}^{d}.

5.2. Results and Discussion

The SVD of the transfer matrix gives the singular values distribution presented in Fig. 8(a). The largest singular value λ_1 is separated by at least 15 dB over the entire bandwidth from the two next ones; apart from the attenuation at the band edges, due to the shape of the time-domain window, the curve is relatively smooth and flat whereas the others present a more noisy behavior.

In order to check that λ_1 is associated to the target we first numerically re-emit in the time-domain the associated singular vector $\tilde{\mathbf{v}}_1$, modified according to our time-domain DORT formulation in Eq. (6), using the same infinitesimal dipole model for the antennas as in the Time Reversal experiment. The resulting movie clearly shows a wave focusing on the target and Fig. 9 is the frame at the instant of best focusing.
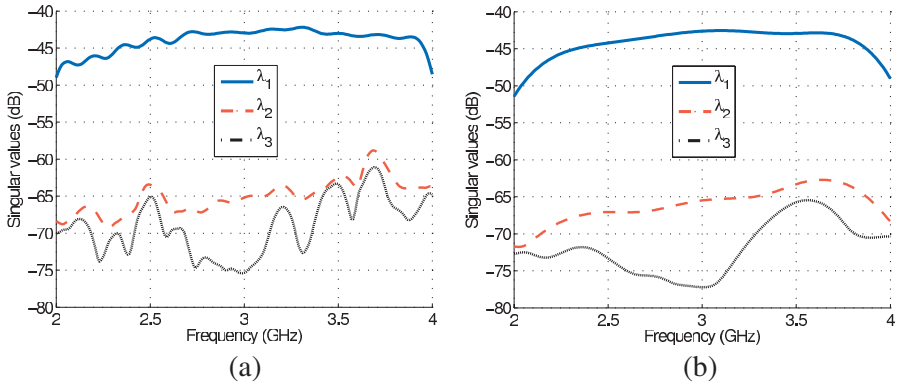
Figure 8. DORT experiment. Three largest singular values distribution versus frequency for the (a) long and (b) short time window cases.
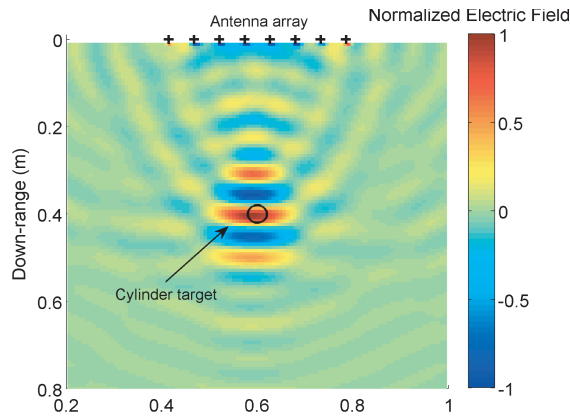

Figure 9. DORT experiment. Numerical time-domain field chart for the singular vector associated to λ_1 in Fig. 8(a) at the instant when the re-emitted wave focuses on the target.

Concerning the smaller singular values, we know from theory [18] that along a line of measurement any extended object also produces anti-symmetric singular vectors, linked to the anisotropic components of the scattered field. These vectors are easily recognizable by one or more phase jumps of nearly 180 deg and magnitude nulls in their complex amplitude distribution. The theoretical computation gives, for the geometry of the problem investigated here, a ratio of about 20–25 dB all over the bandwidth between the first two largest singular

values, associated to the symmetric and the anti-symmetric singular vectors, respectively. While on Fig. 8(a) such a dynamic range is not reached, we get it by gating the $\mathbf{K}^d$ elements with a shorter time-window, 3.5 ns instead of 8.5 ns-long, leading to the singular values distribution on Fig. 8(b). Here the second largest singular value is indeed as smooth as the first one and clearly separated from the third one. For the associated singular vector, the complex amplitude law at 3 GHz with the corresponding monochromatic field chart are presented respectively in Figs. 10(a) and 10(b). On the former, we indeed distinguish a 150 deg phase jump between antennas 4 and 5 and an amplitude decrease of about 15 dB at the same location. The field chart, showing the distribution of the real part of the electric field, has itself a zero around the object position and equal amplitudes but opposite phases with respect to the axis connecting the object and the array center.

A last result is issued from the experimental re-emission in the anechoic chamber of the singular vector $\mathbf{v}_1$ associated to λ_1 in Fig. 8(a). As previously described, the result of the measurement is one single reflection S-parameter per frequency, S_{AA}^d. Recalling that the RF signal is attenuated/phase shifted both before and after propagating in the air (Fig. 7) and exploiting reciprocity, we can write

$$S_{AA}^d = \mathbf{v}_1^T \mathbf{K}^d \mathbf{v}_1 = \mathbf{v}_1^T \mathbf{U} \mathbf{\Lambda} \mathbf{V}^H \mathbf{v}_1 = \lambda_1 \mathbf{v}_1^T \mathbf{u}_1. \tag{14}$$

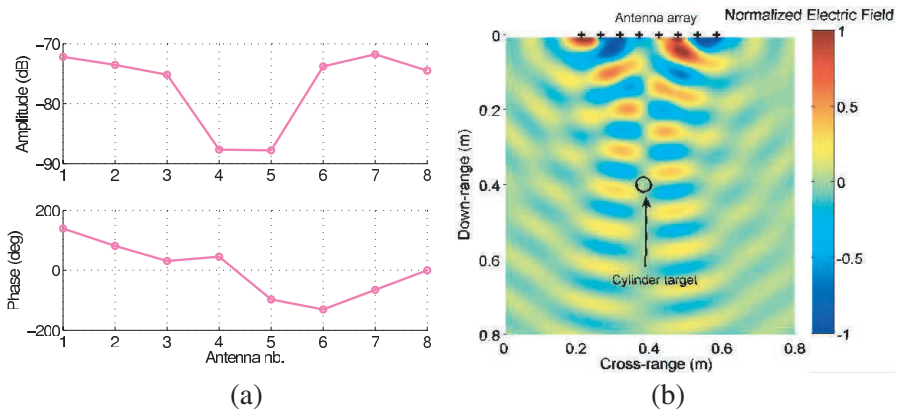In order to further simplify the previous equation we need to write the

Figure 10. DORT experiment. Anti-symmetric singular vector (associated to λ_2 in Fig. 8(b)) (a) complex law and (b) real part of the corresponding monochromatic field chart at 3 GHz.

two singular value problems associated to $\mathbf{K}^{\mathrm{d}}$:

$$\mathbf{K}^{\mathrm{d}}\mathbf{v}_1 = \lambda_1\mathbf{u}_1$$
$$\left(\mathbf{K}^{\mathrm{d}}\right)^T \mathbf{u}_1^* = \lambda_1\mathbf{v}_1^* \tag{15}$$

where $\mathbf{v}_1$ and $\mathbf{u}_1$ are respectively the first right and left singular vectors of $\mathbf{K}^{\mathrm{d}}$. In virtue of reciprocity, $\mathbf{K}^{\mathrm{d}}$ is a symmetric matrix; hence, under the assumption that the dimension of the eigenspace associated to λ_1 is one, which is verified here (Fig. 8), Eq. (15) ensures that $\mathbf{v}_1$ and $\mathbf{u}_1^*$ are colinear. In particular, it exists one particular SVD, called Takagi factorization [32], for which $\mathbf{v}_1 = \mathbf{u}_1^*$. Finally, the development of Eq. (14) simply leads to

$$S_{AA}^{\mathrm{d}} = \lambda_1, \tag{16}$$

that is to say, the DORT singular vector re-emission through the same amplitude/phase law at both transmission and reception allows one to retrieve the corresponding singular value [33].

Nevertheless, our prototype does not allow us to measure exaclty $\lambda_1(\omega)$. $\mathbf{K}^{\mathrm{d}}$ in Eq. (14) is in effect the transfer matrix comprising only the propagation in the air, whereas when we perform the re-emission we also measure twice the propagation through the A/Φ RF channels (made of switches, A/Φ couples fed with $\mathbf{v}_1$, cables and the power splitter to split/recombine the individual signals). If such channels were all strictly identical, a simple amplitude and phase offset should be applied to Eq. (16) to match the measurement result. Unfortunately, due to mismatches between the RF components, the contributions are not the same and the offset cannot be calculated anymore. In order then to verify the quality of our measurement, we rather have to replace $\mathbf{K}$ in Eq. (14) by the actual $\mathbf{K}_{A/\Phi}$ matrix including the propagation through the A/Φ channels, which can be obtained from the measured $\mathbf{K}_{\mathrm{meas}}$ by using the ABCD matrix multiplication technique. The new reference curve is then

$$S_{AA}^{\mathrm{d,ref}}(\omega) = \mathbf{v}_1^T(\omega)\mathbf{K}_{A/\Phi}^{\mathrm{d}}(\omega)\mathbf{v}_1(\omega), \tag{17}$$

which we compare in Fig. 11 against the measured $S_{AA}^{\mathrm{d}}(\omega)$ and which indeed recalls the shape of $\lambda_1(\omega)$ in Fig. 8(a). The error between the curves never exceeds 1–2 dB over the entire bandwidth; as pointed out for the Time Reversal experiment, the main reasons for these discrepancies lie in the finite resolution of the A/Φ couples and in the VNA limited dynamic range.
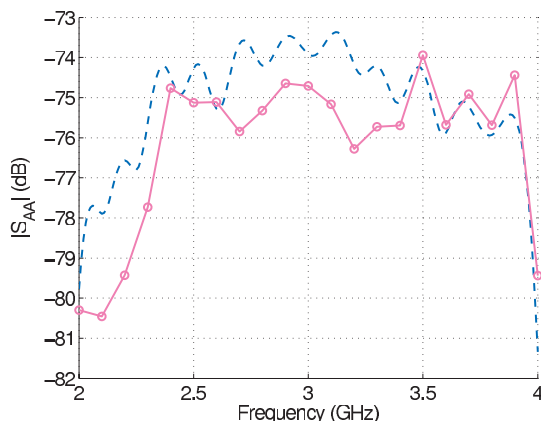
Figure 11. DORT experiment. Amplitude of $S_{AA}^{\mathrm{d}}(\omega)$ measured after re-emission of the singular vector associated to λ_1 in Fig 8(a). The ideal curve is in dashed line, the measurement in full line with circle markers.

6. CONCLUSION

In this paper we have presented a RADAR system able to experimentally perform Phase Conjugation over the whole [2–4] GHz frequency band. Two experiments have validated its behavior by showing an excellent agreement with the expected theoretical results. The first one is the ultrawideband Phase Conjugation of the signal emitted by an active antenna and received by the array; the second one consists in implementing the DORT method to generate a beam focusing on a diffracting object over the entire frequency band. To our best knowledge, the latter is the first experimental report of electromagnetic DORT singular vector re-emission over such a wide frequency band.

We have deliberately opted for an ultrawideband frequency-domain system in contraposition to a time-domain apparatus [11]. In our approach we simultaneously use all the antennas to focus onto the targets at one frequency at the time and finally build the transient focusing beam by the superposition of these time-harmonic waves. The same result can alternatively be obtained by real-time emission of pulses by one antenna at the time, followed by the recombination of these individual pulses. Our choice is mainly motivated by the aim of exploiting the DORT method, which indeed is a frequency-domain technique, within the resolution of inverse problems. Experimental data provided by our RADAR in more complex media shall serve this

purpose.

Finally, the acquisition of a second identical array will add to our prototype interesting features. In particular, the use of two separate arrays will permit us to study the impact of the bistatic angle on clutter rejection and to measure the repsonse of the target to the focusing wave. The latter will be used in the frame of inverse scattering imaging algorithms in order to improve the quality of the reconstructions [4].

REFERENCES

1. Fink, M., C. Prada, F. Wu, and D. Cassereau, "Self focusing in inhomogeneous media with time reversal acoustic mirrors," *Proc. IEEE Ultrasonics Symposium*, Vol. 2, 681–686, 1989.

2. Fink, M., "Time reversal of ultrasonics fields — Part I: Basic principles," *IEEE Trans. Ultrason., Ferroelectr., Freq. Control.*, Vol. 39, 555–566, 1992.

3. Fink, M., D. Cassereau, A. Derode, C. Prada, P. Roux, M. Tanter, J.-L. Thomas, and F. Wu, "Time-reversed acoustics," *Rep. Prog. Phys.*, Vol. 63, No. 12, 1933–1995, 2000.

4. Dubois, A., K. Belkebir, and M. Saillard, "Localization and characterization of two-dimensional targets buried in a cluttered environment," *Inv. Probl.*, Vol. 20, No. 6, S63–S79, 2004.

5. Belkebir, K., M. Saillard, O. Cmielewski, and H. Tortel, "Clutter rejection and inverse scattering," *Proc. Journées de la Matière Condensée*, 210, Toulouse, France, 2006.

6. Belkebir, K., S. Bonnard, F. Pezin, P. Sabouroux, and M. Saillard, "Validation of 2D inverse scattering algorithms from multi-frequency experimental data," *Journal of Electromagnetic Waves and Applications*, Vol. 14, No. 12, 1637–1667, 2000.

7. Liu, X.-F., B.-Z. Wang, S.-Q. Xiao, and J. H. Deng, "Performance of impulse radio UWB communications based on time reversal technique," *Progress In Electromagnetics Research*, Vol. 79, 401–413, 2008.

8. Xiao, S.-Q., J. Chen, X.-F. Liu, and B.-Z. Wang, "Spatial focusing characteristics of time reversal UWB pulse transmission with different antenna arrays," *Progress In Electromagnetics Research B*, Vol. 2, 223–232, 2008.

9. Maaref, N., P. Millot, X. Ferrières, C. Pichot, and O. Picon, "Electromagnetic imaging method based on time reversal processing applied to through-the-wall target localization," *Progress In Electromagnetics Research M*, Vol. 1, 59–67, 2008.

10. Zheng, W., Z. Zhao, Z.-P. Nie, and Q. H. Liu, "Evaluation of

TRM in the complex through wall environment," *Progress In Electromagnetics Research*, Vol. 90, 235–254, 2009.

11. Lerosey, G., J. de Rosny, A. Tourin, A. Derode, and M. Fink, "Time reversal of wideband microwaves," *Appl. Phys. Lett.*, Vol. 88, No. 15, 154101, 2006.

12. Lerosey, G., J. de Rosny, A. Tourin, A. Derode, G. Montaldo, and M. Fink, "Time reversal of electromagnetic waves," *Phys. Rev. Lett.*, Vol. 92, No. 19, 193904, 2004.

13. Khaleghi, A., G. El Zein, and I. Naqvi, "Demonstration of time-reversal in indoor ultra-wideband communication: Time domain measurement," *Proc. IEEE International Symposium on Wireless Communication Systems*, 465–468, Trondheim, Norway, 2007.

14. Liu, D., S. Vasudevan, J. Krolik, G. Bal, and L. Carin, "Electromagnetic time-reversal source localization in changing media: Experiment and analysis," *IEEE Trans. Antennas Propag.*, Vol. 55, No. 2, 344–354, 2007.

15. Cresp, A., I. Aliferis, M. J. Yedlin, J.-Y. Dauvignac, and C. Pichot, "Time-domain processing of electromagnetic data for multiple-target detection," *AIP Conf. Proc., 3rd Conference on Mathematical Modeling of Wave Phenomena*, Vol. 1106, No. 1, 204–213, 2009.

16. Prada, C. and M. Fink, "Eigenmodes of the time reversal operator: A solution to selective focusing in multiple-target media," *Wave Motion*, Vol. 20, 151–163, 1994.

17. Tortel, H., G. Micolau, and M. Saillard, "Decomposition of the time reversal operator for electromagnetic scattering," *Journal of Electromagnetic Waves and Applications*, Vol. 13, No. 5, 687–719, 1999.

18. Micolau, G. and M. Saillard, "D.O.R.T. method as applied to electromagnetic subsurface sensing," *Radio Sci.*, Vol. 38, No. 3, S63–S79, 2003.

19. Chambers, D. H. and A. K. Gautesen, "Analysis of the time-reversal operator for a small spherical scatterer in an electromagnetic field," *IEEE Trans. Antennas Propag.*, Vol. 52, No. 7, 1729–1738, 2004.

20. Derode, A., P. Roux, and M. Fink, "Robust acoustic time reversal with high-order multiple scattering," *Phys. Rev. Lett.*, Vol. 75, No. 23, 4206–4209, 1995.

21. Draeger, C. and M. Fink, "One-channel time reversal of elastic waves in a chaotic 2d-silicon cavity," *Phys. Rev. Lett.*, Vol. 79, No. 3, 407–410, 1997.

22. Kuperman, W. A., W. S. Hodgkiss, H. C. Song, T. Akal, C. Ferla, and D. R. Jackson, "Phase Conjugation in the ocean: Experimental demonstration of an acoustic time-reversal mirror," *J. Acoust. Soc. Amer.*, Vol. 103, 25–40, 1998.

23. Mordant, N., C. Prada, and M. Fink, "Highly resolved detection and selective focusing in a waveguide using the D.O.R.T. method," *J. Acoust. Soc. Amer.*, Vol. 105, No. 5, 2634–2642, 1999.

24. Yavuz, M. E. and F. L. Teixiera, "Space-frequency ultrawideband time-reversal imaging," *IEEE Trans. Geosci. Remote Sens.*, Vol. 46, No. 4, 115–1124, 2008.

25. Philippe, F. D., C. Prada, D. Clorennec, M. Fink, and T. Folégot, "Construction of the temporal invariants of the time-reversal operator," *J. Acoust. Soc. Amer. Express Letters*, Vol. 126, No. 1, EL8–EL13, 2009.

26. Micolau, G., M. Saillard, and P. Borderies, "DORT method as applied to ultrawideband signals for detection of buried objects," *IEEE Trans. Geosci. Remote Sens.*, Vol. 41, No. 8, 1813–1820, 2003.

27. Stewart, G. W., *Matrix Algorithms-volume II: Eigensystems*, *SIAM*, Philadelphia, New York, 1998.

28. Borcea, L., G. Papanicolaou, C. Tsogka, and J. Berryman, "Imaging and time reversal in random media," *Inv. Prob.*, Vol. 18, No. 5, 1247–1279, 2002.

29. Guillanton, E., J. Y. Dauvignac, C. Pichot, and J. Cashman, "A new design tapered slot antenna for ultra-wideband applications," *Microwave and Optical Technology Letters*, Vol. 19, No. 4, 286–289, 1998.

30. Pozar, D. M., *Microwave Engineering*, John Wiley & Sons, Toronto, 1998.

31. Derode, A., A. Tourin, and M. Fink, "Time reversal versus phase conjugation in a multiple scattering environment," *Ultrasonics*, Vol. 40, 275–280, 2002.

32. Horn, R. A. and C. R. Johnson, *Matrix Analysis*, Cambridge University Press, Cambridge, 1985.

33. Borcea, L., G. Papanicolaou, and C. Tsogka, "Optimal waveform design for array imaging," *Inv. Probl.*, Vol. 23, No. 5, 1973–2020, 2007.